ResearchGate

See discussions, stats, and author profiles for this publication at: https://www.researchgate.net/publication/231709960

Light-Scattering Study of Diblock Copolymers in Supercritical Carbon Dioxide: CO2 Density-Induced Micellization Transition

ARTICLE *in* MACROMOLECULES · OCTOBER 1998

Impact Factor: 5.8 · DOI: 10.1021/ma980442j

CITATIONS
70

READS
36

4 AUTHORS, INCLUDING:

Eric Buhler
Paris Diderot University
61 PUBLICATIONS **1,351** CITATIONS
SEE PROFILE

Andrey V Dobrynin
University of Akron
124 PUBLICATIONS **4,912** CITATIONS
SEE PROFILE

Michael Rubinstein
University of North Carolina at Chapel Hill
103 PUBLICATIONS **4,899** CITATIONS
SEE PROFILE

Available from: Andrey V Dobrynin
Retrieved on: 27 January 2016

Light-Scattering Study of Diblock Copolymers in Supercritical Carbon Dioxide: CO_2 Density-Induced Micellization Transition

E. Buhler, A. V. Dobrynin, J. M. DeSimone,* and M. Rubinstein*

Venable and Kenan Laboratories, Department of Chemistry CB#3290, University of North Carolina at Chapel Hill, Chapel Hill, North Carolina 27599-3290

Received March 20, 1998; Revised Manuscript Received August 17, 1998

ABSTRACT: The behavior of polymeric surfactant polyvinyl acetate (PVAC)-*b*-poly(1,1,2,2-tetrahydroperfluorooctyl acrylate) (PTAN) in supercritical carbon dioxide (CO_2) was investigated using static and dynamic light scattering. We observed three regions on the phase diagram of the copolymer in supercritical CO_2: (i) two-phase region at low CO_2 density; (ii) solutions of spherical micelles at intermediate CO_2 densities; (iii) solutions of unimers (individual copolymer chains) at high CO_2 densities. The aggregation number (the number of copolymer chains in a micelle) decreases with an increasing density of supercritical CO_2 in region (ii). An increase of the CO_2 density corresponds to the improvement of solvent quality for both blocks of the copolymer (PVAC and PTAN). The hydrodynamic radius of micelles and unimers was measured using dynamic light scattering in regions (ii) and (iii), respectively. This light-scattering study is the first one reporting a solvent density-induced transition between spherical micelles at lower supercritical CO_2 density and unimers at higher CO_2 density. The light-scattering technique appears to be a very powerful tool for the analysis of the carbon dioxide density-induced micellization transition. This phenomenon is unique to supercritical fluids and demonstrates a convenient control over the polymer solubility.

1. Introduction

Carbon dioxide aided by "smart" molecules, such as surfactants and block and dendritic polymers will affect a wide range of industries. More than 30 billion pounds of organic and halogenated solvents are used worldwide each year as process aids, cleaning agents, and dispersants. Solvent industries such as aerospace, automotive, chemical, electronics, food, petroleum, pharmaceutical, and pulp and paper textiles need to consider alternatives that can reduce or eliminate the negative impact that solvent emissions have on our environment. Carbon dioxide provides an attractive solvent alternative for a variety of chemical and industrial manufacturing processes, because of its low cost, wide availability, moderate critical conditions (critical temperature T_c = 31 °C, critical pressure P_c = 73.8 bar, and critical density ρ_c = 0.468 g/cm^3), and environmentally and chemically benign nature.[1]

However only a few classes of polymeric materials (fluoropolymers and silicones[2−5]) are soluble in supercritical carbon dioxide at relatively mild conditions (T < 100 °C, P < 350 bar), while conventional polymers with hydrophobic, hydrophilic, or lipophilic groups are relatively insoluble. Development of amphiphilic molecules for the use as surfactants in supercritical CO_2 and other supercritical fluids has led to the study of micellar and microemulsion phases in supercritical fluid media.[6−9] A strategy is to use diblock copolymers. These diblock copolymers are composed of chain segments with dissimilar solubility characteristics and can self-assemble into micelles when placed in supercritical carbon dioxide. Their self-assembly into micelles in supercritical CO_2 has already been demonstrated by small-angle neutron-scattering experiments.[10] Dynamic light scattering was used to investigate steric stabilization and flocculation of dilute poly(2-ethylhexyl acrylate) emulsions in the liquid CO_2 by monitoring changes in droplet size over time at various CO_2 densities.[11]

In the present paper we report the results of the light-scattering experiments performed on the supercritical solutions of poly(1,1,2,2-tetrahydroperfluorooctyl acrylate)-*b*-poly(vinyl acetate) (PTAN (60.4k g/mol)-*b*-PVAC (10.3k g/mol) for copolymer concentrations ranging from $c = 2.3 \times 10^{-4}$ g/cm^3 to $c = 0.02$ g/cm^3 and at CO_2 densities from $\rho = 0.8$ g/cm^3 to $\rho = 1$ g/cm^3. We have identified three regions on the phase diagram in the copolymer concentration−CO_2 density plane at a fixed temperature (T = 45 °C): (i) Two-phase region at low CO_2 density; (ii) spherical micelles at intermediate CO_2 density; (iii) unimers (isolated copolymer chains) dissolved in CO_2 at high density.

In section 2 of the paper we describe materials and experimental techniques used in this study. In section 3 we report the results of the experiments.

2. Materials and Methods

2.1. Sample Characteristics. We have investigated a diblock copolymer containing a carbon dioxide-phobic moiety, poly(vinyl acetate) (PVAC, 10.3 kg/mol), and a carbon dioxide-philic block, poly(1,1,2,2-tetrahydroperfluorooctyl acrylate) (PTAN, 60.4 kg/mol)[12] in supercritical CO_2 as a function of copolymer concentration and carbon dioxide density (pressure). Because of the solubility differences in carbon dioxide, such block copolymers are predisposed to self-assemble into micellular structures.[10] The sample was weighed into the preparation view cell before adding the carbon dioxide. Each intensity measurement was taken after a period of time greater than 5 min when the temperature and pressure became constant. The solutions were investigated in the copolymer concentration range (2.3×10^{-4})−0.02 g/cm^3 at the temperature T = 45 °C and in the CO_2 density range 0.8−1 g/cm^3 (pressure range of 180−550 bar).

We have also carried out static light scattering from CO_2 solutions of a 36.5 kg/mol poly(1,1-dihydroperfluorooctyl acrylate) homopolymer and of poly(vinyl acetate) homopolymers

* To whom correspondence should be addressed.

10.1021/ma980442j CCC: $15.00 © 1998 American Chemical Society
Published on Web 09/25/1998

(5.8, 16.64, and 46.34 kg/mol). Poly(1,1-dihydroperfluorooctyl acrylate) homopolymer and poly(1,1,2,2-tetrahydroperfluorooctyl acrylate) homopolymer (PTAN) have a very similar chemical structure. Moreover, cloud point measurements indicate that both homopolymers have the same solubility characteristics in supercritical CO_2[12,13] (see part 3.1.1.).

2.2. Static Light Scattering. Static light scattering (SLS) and dynamic light scattering (DLS) experiments were performed by means of a spectrometer equipped with an argon ion laser (Coherent Innova 70-3) operating at $\lambda = 514$ nm, a BI9000 correlator from Brookhaven Instruments, and a computer-controlled and stepping-motor-driven variable angle detection system. The scattering spectrum was measured through a band-pass filter (514.5 nm) and a pinhole (200 μm for the static experiments and 50 μm for the dynamic experiments) with a photomultiplier tube (BI-PMT9836).

In the SLS experiments one measures the excess of scattered intensity $I(q)$ with respect to the solvent, where the magnitude of the scattering wave vector q is given by

$$q = \frac{4\pi n}{\lambda} \sin\frac{\theta}{2} \tag{1}$$

In eq 1 n is the refractive index of the solvent, λ is the wavelength of light in the vacuum, and θ is the scattering angle. The refractive[14,15] index was calculated from the virial equation for the molar refractivity of the carbon dioxide at 45 °C. Corrections to the absolute scattering intensities $I(q)$ (i.e., excess Rayleigh ratio) were made using a toluene sample reference for which the excess Rayleigh ratio is well-known.

Plots of $c/I(q)$ versus q^2 were extrapolated to $q = 0$ to give intercepts $c/I(0)$. In dilute solutions, the average radius of gyration R_G can be determined from the intercept and the slope of these plots using a scattering inverse Lorentzian law of the form[16]

$$\frac{c}{I(q)} = \frac{c}{I(0)}\left[1 + \frac{q^2 R_G{}^2}{3}\right] \tag{2}$$

In our experiments the size of the copolymer aggregates and of the polymers was too small to see a q^2 dependence, so the experiments were done at $\theta = 90°$. One can use a virial expression for the osmotic pressure to deduce the weight-average molecular weight[16] M_W

$$I(0) = KcM_W(1 - 2A_2cM_W + ...) \tag{3}$$

where A_2 is the second virial coefficient which describes the polymer−solvent interactions. The scattering constant is $K = 4\pi^2 n^2 (dn/dc)^2/N_A\lambda^4$ where dn/dc is the refractive index increment and N_A is Avogadro's number.

2.3. Dynamic Light Scattering. In the dynamic light-scattering (DLS) experiments, the normalized time autocorrelation function $g^{(2)}(q,t)$ of the scattered intensity is measured.[16]

$$g^{(2)}(q,t) = \frac{\langle I^*(q,0)\, I(q,t)\rangle}{\langle I^*(q,0)\rangle^2} \tag{4}$$

The latter can be expressed in terms of the field autocorrelation function or equivalently in terms of the autocorrelation function of the concentration fluctuations $g^{(1)}(q,t)$ through

$$g^{(2)}(q,t) = A + \beta|g^{(1)}(q,t)|^2 \tag{5}$$

where A is the baseline and β the coherence factor which in our experiments is equal to 0.7−0.9. The normalized dynamical correlation function $g^{(1)}(q,t)$ of polymer concentration fluctuations is defined as

$$g^{(1)}(q,t) = \frac{\langle \delta c^*(q,0)\, \delta c(q,t)\rangle}{\langle \delta c(q,0)^2\rangle} \tag{6}$$

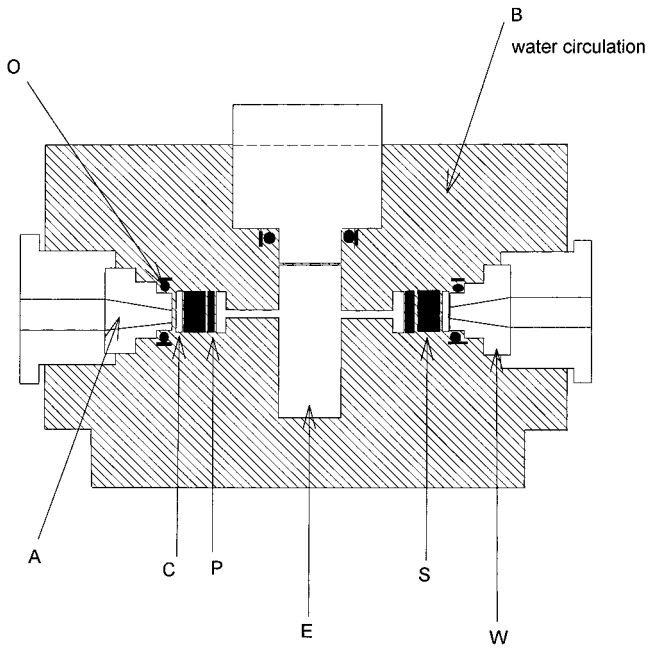

Figure 1. High-pressure optical cell: (A) window aperture; (B) cell body; (C) copper O-ring; (E) sample emplacement; (O) viton O-ring; (P) plastic O-ring; (S) sapphire window; (W) window support. Windows at 45°, 90° and 135° are omitted for clarity.

where $\delta c(q,t)$ and $\delta c(q,0)$ represent fluctuations of the polymer concentration at time t and zero, respectively.

In our experiments, the inspection of the angular dependence shows that the relaxation is diffusive with characteristic time inversely proportioned to q^2. Some of our dilute solutions were characterized by a single relaxation mechanism. For these solutions we have adopted the classical cumulant analysis.[17] This analysis provides the variance of the correlation function and the first reduced cumulant $(\tau q^2)^{-1}$ where τ is the average relaxation time of $g^{(1)}(q,t)$. The extrapolation of $(\tau q^2)^{-1}$ to $q = 0$ yields the values of the mutual diffusion constant D. The latter is related to the average hydrodynamic radius R_H of the micelles and of the free copolymers trough

$$D = \frac{kT}{6\pi\eta_s R_H} \tag{7}$$

where k is the Boltzmann constant, η_s the carbon dioxide viscosity, and T the absolute temperature. To determine the carbon dioxide viscosity, which depends on the density and the temperature, we were using the relation developed by H. Sovoná et al.[18] In our experiments the CO_2 viscosity is varying from 0.05 to 0.15 cP in the CO_2 density interval from 0.8 to 1 g/cm^3 at $T = 45$ °C.

We also used another method to determine τ: the Contin method based on the inverse Laplace transform of $g^{(1)}(q,t)$.[19] If the spectral profile of the scattered light can be described by a multi-Lorentzian curve, then $g^{(1)}(q,t)$ can be written as

$$g^{(1)}(q,t) = \int_0^\infty G(\Gamma)\exp(-\Gamma t)\, d\Gamma \tag{8}$$

where $G(\Gamma)$ is the normalized decay constant distribution. This method is more appropriate for solutions characterized by several relaxation mechanisms (e.g., mixture of micelles and unimers).

2.4. High-Pressure Setup. Sample measurements were performed using an 8.5-mL high-pressure optical cell[20,21] shown schematically in Figure 1. The cell was designed to operate at pressures up to 4 kbar and was constructed to fit on the top of a BI-200SM goniometer without modification. The high-pressure cell was constructed from alloy tool steel and heat-treated for strength. The cylindrical cell body (B) has an axial

Table 1. Variation of the Excluded Volume Parameter and of the Second Virial Coefficient As a Function of the CO_2 Density for a 36.5 kg/mol Poly(1,1-dihydroperfluorooctyl acrylate) Sample at $T = 45$ °C (Note That the Volume of a Monomer Is Equal to 538 Å^3)

CO_2 density ρ (g/cm^3)	pressure P (bar)	second virial coefficient A_2 (cm^3·g^{-2}·mol)	excluded volume parameter v (Å^3)
0.84	207	$(3.86 \pm 1) \times 10^{-5}$	26.4
0.88	276	$(2.19 \pm 1) \times 10^{-4}$	150
0.92	345	$(3.58 \pm 1) \times 10^{-4}$	245
0.95	414	$(4.42 \pm 1) \times 10^{-4}$	303

hole which holds the sample volume (E). Three windows located at 45°, 90°, and 135° relative to the incident beam can be used for scattering measurements while windows at 0° and 180° served as the entrance and exit windows for the light source. Each angular port (W) was fitted with a sapphire window (S) (length 8 mm, diameter 11 mm, Hemex quality) from Crystal Systems of Salem, MA. The window aperture was around 5 mm in diameter. In this geometry, the optical axis of the sapphire (001) was coincident with the direction of the incident and scattered light. Temperature was measured with a resistive temperature device located in close proximity (around 2 cm) to the sample (a water circulation in the body of the cell was used for the control of the temperature). Temperature control was provided by a Lauda temperature bath which gave a temperature stability of ±0.2 °C.

The light scattering cell was connected to a 25-mL magnetically stirred view cell. The carbon dioxide, injected into the preparation view cell, was filtered using a 0.5-μm porous metal filter (High Pressure Equipment Co.). The carbon dioxide was pressurized using an ISCO pump and the pressure was measured with a pressure transducer (Sensotoc TJF/743-11).

3. Experimental Results and Discussion

3.1. Effect of the Carbon Dioxide Density. 3.1.1. Solution Properties of the CO_2-Soluble Fluoropolymer. We have carried out static light scattering from CO_2 solution of a 36.5 kg/mol poly(1,1-dihydroperfluorooctyl acrylate) homopolymer. We measured the dependence of the second virial coefficient in the CO_2 range $0.84 < \rho < 0.95$ g/cm^3 at a temperature $T = 45$ °C using the method described in section 2.2 above. The variation of the second virial coefficient A_2 and of the excluded volume parameter v for a fluoro homopolymer poly(1,1-dihydroperfluorooctyl acrylate) at $T = 45$ °C with CO_2 density is illustrated in Table 1. The positive sign of the second virial coefficients indicates that at these conditions the CO_2 medium is a good solvent for the fluoropolymer (PTAN). Actually, the value of the second virial coefficient is increasing with the CO_2 pressure or density. These results suggest that the quality of the solvent is improving with increasing CO_2 density. A similar trend in the dependence of the second virial coefficient of fluoropolymers on the carbon dioxide pressure was observed in previous scattering experiments.[22] A similar effect of the pressure on the solvent quality was also observed by a fluorescent probe method.[11]

Cloud point measurements for the poly(1,1-dihydroperfluorooctyl acrylate) and for the poly(1,1,2,2-tetrahydroperfluorooctyl acrylate) (PTAN) were done at 45 °C. The cloud point is defined as the point where the solution turned completely transparent (visually) as the pressure was slowly increased.[12,13] Each cloud point condition was repeated several times with reproducibility within ±2 bar. For a given molecular weight, solubility characteristics are the same for both homopolymers within an error bar of 5%.[12,13]

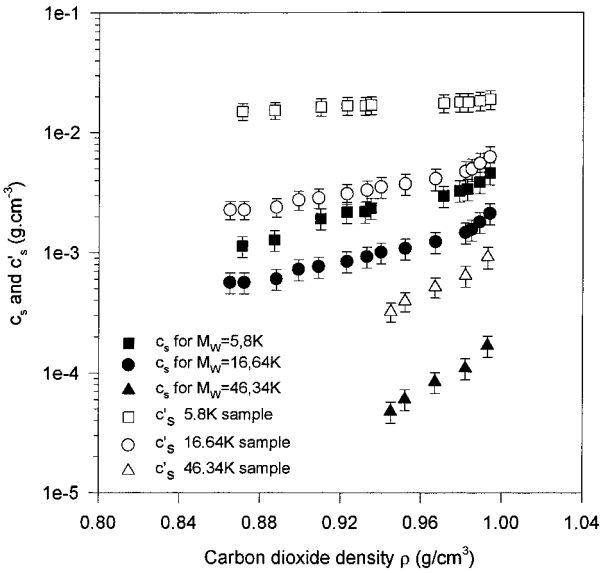

Figure 2. CO_2 density dependence at $T = 45$ °C of the supernatant concentration c_s of three poly(vinyl acetate) samples having molecular weights equal to 5.8 kg/mol (■), 16.64 kg/mol (●), and 46.34 kg/mol (▲) (assuming no preferential solubility). Solubility measurements were performed using static light-scattering experiments. The open symbols give the corresponding concentrations of the supernatant c_s' determined using the analysis of the GPC data (see text for details).

3.1.2. Poly(vinyl acetate) Solubility Measurements. The quality of supercritical carbon dioxide as a solvent for poly(vinyl acetate) (PVAC) blocks depends on the CO_2 pressure (or on the CO_2 density). To quantify this feature, the solubility of the PVAC of different molecular weights ($M_W = 5.8$, 16.64, and 46.34 kg/mol) was measured as a function of CO_2 density between 0.84 and 1 g/cm^3 (see Figure 2). The PVAC concentration in the dilute phase (saturated solution) was deduced from the scattered intensity $I(q)$ at a fixed angle (90°) using a known polymer molecular weight.[23] Neglecting the second virial term in eq 3, this concentration c_s of the supernatant was approximated by

$$c_s = \frac{I(q \to 0)}{KM_W} \approx \frac{I(q)}{KM_W} \tag{9}$$

To perform these solubility measurements, filtered-pressured carbon dioxide was added to a large amount of polymers ($c > 0.028$ g/cm^3). The measurements were performed once equilibrium scattered intensity was reached (see Figure 2). These measurements show the increase of the solvent quality for the PVAC block with increasing CO_2 density and clarify the mechanism of the micelles-to-unimers transition described below. As expected, the solubility is higher for lower molecular weight polymers. The experiments could not be performed below a certain CO_2 density (that depends on PVAC molecular weight) because the intensity scattered by the polymer was of the order of the experimental error.

Actually, the polydispersity of all three sample was quite high (i.e., the degree of polydispersity was equal to 1.45, 1.455, and 1.53 for the weight-average molecular weight 5.8, 16.64, and 46.34 kg/mol samples, respectively). To evaluate the real concentration c_s' and the real molecular weight of the polymer molecules dissolved in the carbon dioxide, we used the gel permeation

chromatography (GPC) data. Consider a polymer of molecular weight M from the distribution. These chains in the dilute phase (saturated supernatant phase) at concentration $c_s'(M)$ are in equilibrium with the same chains in the sediment at concentration $c'(M)$. The input fraction of chains with molecular weight M (the input average concentration $c_0(M)$ is divided between the sediment occupying fraction x of the cell volume and the supernatant in the remaining fraction $1 - x$ of cell volume.

$$xc'(M) + (1 - x)c_s'(M) = c_0(M) \tag{10}$$

The value of x was evaluated self-consistently by taking into account the mass of the sediment and its density. We started from the initial value of x = 0.028 and made several iterations until the solution reached the fixed point (saturated) at a self-consistent value of x. The energy penalty paid by a chain of molecular weight M for leaving the sediment and entering the supernatant in the form of a globule is the surface energy of the globule γA(M), where γ is the surface tension between PVAC and CO_2 and A(M) the surface area of the globule. The reduction of the concentration of the molecules of molecular weight M in the supernatant with respect to the sediment is

$$c_s'(M) = c'(M) \exp\left[\frac{-\gamma A(M)}{kT}\right] \tag{11}$$

The area $A(M)$ of the globule can be estimated from a simple scaling picture of the dense packing of thermal blobs[24] of size ξ_{th} containing g_{th} monomers

$$g_{th} \approx \left(\frac{\xi_{th}}{b}\right)^2 \tag{12}$$

where b is the size of the monomer. The size of the globule is

$$R \approx \xi_{th}\left(\frac{M}{g_{th}m_0}\right)^{1/3} \approx \left(\xi_{th}\frac{M}{m_0}b^2\right)^{1/3} \tag{13}$$

where m_0 is the molecular weight of a monomer and M/m_0 is the degree of polymerization. The surface tension γ of the PVAC−CO_2 interface is of the order of the thermal energy kT per thermal blob at the surface of the globule.

$$\gamma \approx \frac{kT}{\pi\xi_{th}^2} \tag{14}$$

Therefore, the thermal blob size is

$$\xi_{th} \approx \left(\frac{kT}{\pi\gamma}\right)^{1/2} \tag{15}$$

The area of the globule of molecular weight M is

$$A(M) = 4\pi R^2(M) = 4\pi\left(\frac{kT}{\pi\gamma}\right)^{1/3}\left(\frac{Mb^2}{m_0}\right)^{2/3} \tag{16}$$

The fraction of molecules of molecular weight M present in the cell at the input average concentration $c_0(M)$ is defined as

$$c_0(M) = c_0 f(M) \tag{17}$$

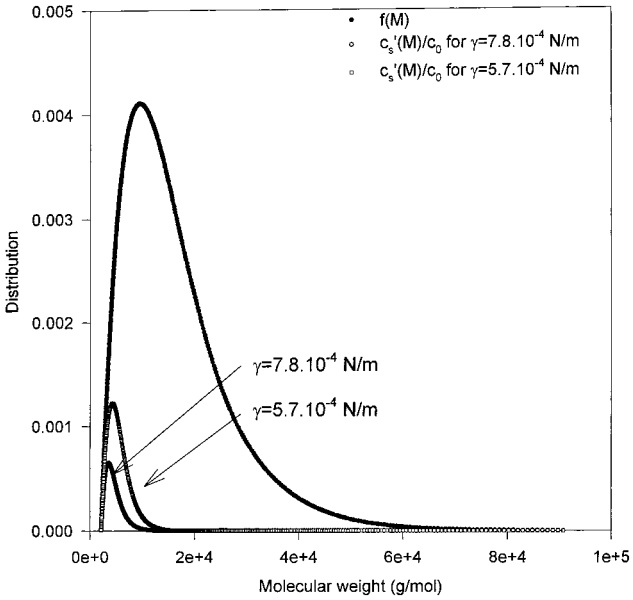

Figure 3. Normalized molecular weight distribution *f(M)* of a PVAC homopolymer block with a weight-average molecular weight equal to 16.64 kg/mol. Molecular weight distribution of the soluble fractions $c_s'(M)/c_0$ calculated for two surface tensions are also plotted.

Here, *f(M)* denotes the input fraction of polymers with molecular weight M and c_0 denotes the total input polymer concentration (i.e., 0.028 g/cm^3). The function *f(M)* is normalized

$$\int_0^\infty f(M)\frac{dM}{m_0} = 1 \tag{18}$$

So, that sum of all input concentrations $c_0(M)$ over all molecular weight fractions is the total input concentration c_0.

$$\int_0^\infty c_0(M)\frac{dM}{m_0} = c_0 \tag{19}$$

Therefore, the soluble polymer concentration (concentration of the supernatant) c_s' at a surface tension γ is given by

$$c_s' = \int_0^\infty c_s'(M)\frac{dM}{m_0} = \int_0^\infty \frac{c_0(M)\frac{dM}{m_0}}{x\exp\left[\frac{\gamma A(M)}{kT}\right] + 1 - x} \tag{20}$$

The weight-average molecular weight of the dissolved fraction M_W' is equal to

$$M_W' = \frac{\int_0^\infty c_s' M^2\, dM}{\int_0^\infty c_s' M\, dM} \tag{21}$$

Figure 3 shows the GPC distribution *f(M)* for a PVAC sample with the weight-average molecular weight M_W = 16.64 kg/mol. In Figure 3 is also plotted $c_s'(M,\gamma)/c_0$ for two values of the interfacial tension γ: 7.8×10^{-4} and 5.7×10^{-4} N/m. As the surface tension increases, the dissolved fraction becomes smaller and shifts to the lower molecular weights. For example, for $\gamma = 7.8 \times 10^{-4}$ N/m ($x = 0.06$ and the sediment density is equal

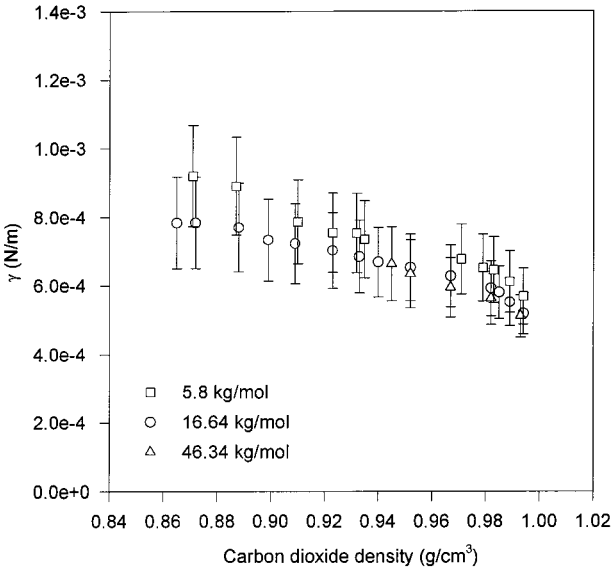

Figure 4. Interfacial tension evaluated using GPC and static light-scattering experiments as a function of CO_2 density for three PVAC samples: 5.8 (□), 16.64 (○) and 46.34 (△) kg/mol.

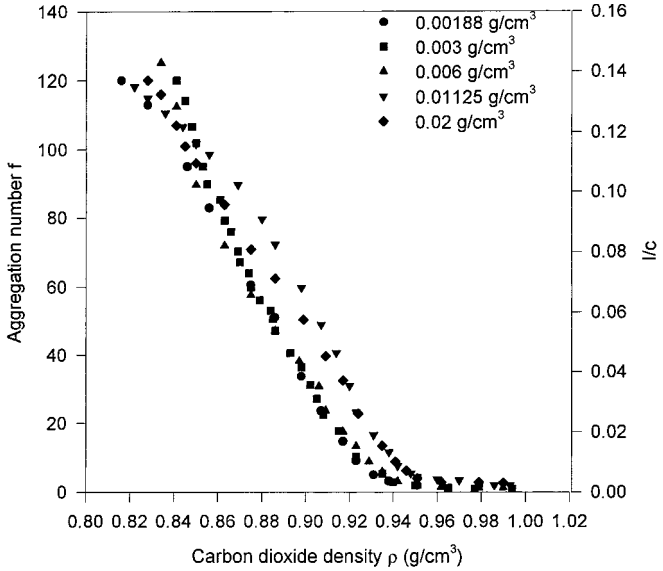

Figure 5. Variation of the absolute scattered intensity I divided by the copolymer concentration c and of the aggregation number f with the CO_2 density at $T = 45$ °C for five copolymer concentrations: $c = 1.88 \times 10^{-3}$, 3×10^{-3}, 6×10^{-3}, 1.125×10^{-2}, and 2×10^{-2} g/cm^3. The experimental error is equal to 20%.

to 0.43 g/cm^3), we found the following estimates of the concentration of supernatant: $c_s' = 2.35 \times 10^{-3}$ g/cm^3 and the weight-average molecular weight of the supernatant $M_W' = 4650$ g/mol, which is significantly different from the weight-average molecular weight of the input sample. The ratio $M_W/M_W' = 3.6$ quantitatively characterizes the fractionation of the polydisperse sample by selective solubility of the lower molecular weight fraction in the supercritical CO_2.

The product $c_s'M_W'$ for the soluble fraction of the sample (supernatant) is proportional to the scattered intensity and can be compared to the experimental one (see eq 9).

$$c_s'M_W' = \frac{I(0)}{K} \tag{22}$$

The product $c_s'M_W'$ is a function of γ and it is easy to evaluate the surface tension for each experimental scattered intensity and therefore for each CO_2 density ρ. In Figure 4 the calculated surface tension is plotted as a function of the carbon dioxide density for the three samples (5.8, 16.64, and 46.34 kg/mol). The decrease of the surface tension with increasing of the CO_2 density is a direct consequence of the improving solvent quality. Note that the surface tension is molecular-weight-independent. A similar trend in the dependence of the surface tension on the CO_2 density was observed for poly(2-ethylhexyl acrylate).[25] The open symbols in Figure 2 give the corresponding concentrations of the supernatant. These concentrations c_s' are significantly higher than the concentration c_s obtained directly from the scattered intensity assuming no difference in composition between the sediment and supernatant (from eq 9). The CO_2 fractionation factor M_W/M_W' for these samples varies in the range 2.5−3.6 with decreasing CO_2 density.

3.1.3. Aggregation Number. Large insoluble aggregates in suspension were observed at densities below $\rho = 0.814$ g/cm^3 and were interpreted as a signature of a two-phase solution. We report our measurements at CO_2 densities above the cloud line ($\rho \sim 0.814$ g/cm^3 at $T = 45$ °C).

The standard approximation[23,26,27] to determine the aggregation number f is to take the ratio of the average mass of the micelle $M_{micelles}$ deduced from the scattered intensity I/c extrapolated to a zero wavevector (see Figure 5), to the mass of a copolymer chain $M_{unimers}$ (70.7 kg/mol):

$$f = \frac{M_{micelles}}{M_{unimers}} \tag{23}$$

where the mass of micelles is

$$M_{micelles} = \frac{I(0)}{Kc} \tag{24}$$

In this analysis, the effect of the second virial coefficient between the micelles is neglected. The concentration of free copolymers present in the micellar solution is expected to be of the order of the CMC (critical micelle concentration), and their contribution to the scattered intensity is also neglected in the determination of the micellar mass (eq 24). In section 3.3 below we demonstrate that this approximation fails near the micelles-to-unimers transition.

In Figure 5, the aggregation number measured at $T = 45$ °C is plotted as a function of the carbon dioxide density for the five surfactant concentrations: 1.88×10^{-3}, 3×10^{-3}, 6×10^{-3}, 1.125×10^{-2}, and 2×10^{-2} g/cm^3. The curves exhibit a decrease of the aggregation number from 120 to 1 with increasing CO_2 density. For example, the unimers phase was reached when the aggregation number f is equal to 1 for CO_2 density around 0.95 g/cm^3 for polymer concentration $c = 1.125 \times 10^{-2}$ g/cm^3. The decrease of the aggregation number with an increasing CO_2 density is a direct consequence of the improving solvent quality. As shown in Table 1, Figure 2, and Figure 4, the solvent quality is improving for both blocks of the diblock copolymer. Our results indicate the existence of the CO_2 density-induced transition between the spherical micellar phase and the unimer (free copolymer chains) phase.

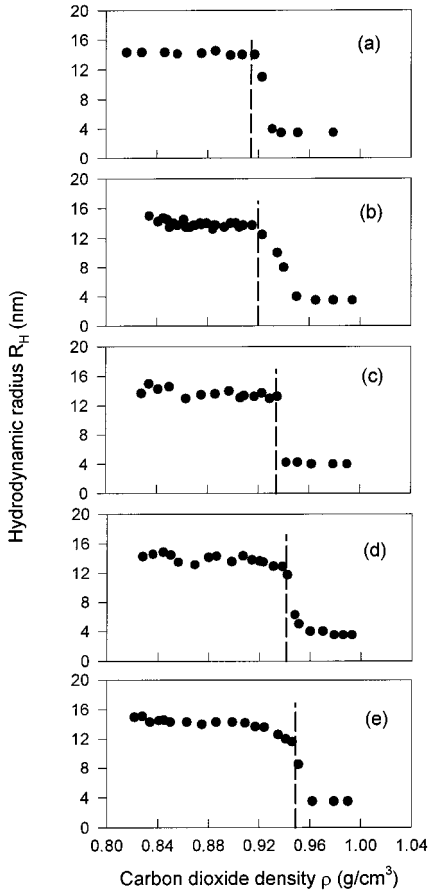

Figure 6. Effect of the CO_2 density on the hydrodynamic radius (determined with the cumulant analysis) for a copolymer concentration: (a) $c = 1.88 \times 10^{-3}$ g/cm^3, (b) $c = 3 \times 10^{-3}$ g/cm^3, (c) $c = 6 \times 10^{-3}$ g/cm^3, (d) $c = 1.125 \times 10^{-2}$ g/cm^3, and (e) $c = 2 \times 10^{-2}$ g/cm^3 at temperature $T = 45$ °C. Dashed lines indicate the onset of the micelles-to-unimers transition as determined by the Contin analysis of the dynamic light-scattering data. Error bars are equal to the size of the points.

3.2. Hydrodynamic Radius and Phase Diagram.

From the dynamic light-scattering data, we have determined the translational diffusion coefficient D, the hydrodynamic radius R_H, and the particle size distribution. The hydrodynamic radius over the CO_2 density range of 0.8−1 g/cm^3 for the PTAN-*b*-PVAC diblock copolymer solution at $T = 45$ °C for the different copolymer concentrations 1.88×10^{-3}, 3×10^{-3}, 6×10^{-3}, 1.125×10^{-2}, and 2×10^{-2} g/cm^3 is presented in Figure 6. For example, the micellar aggregates with the radius $R_H \approx 15.3 \pm 1$ nm were observed in the CO_2 density range 0.82 g/cm^3 < ρ <0.91 g/cm^3 for copolymer concentration of $c = 0.003$ g/cm^3. The size of the micelles is almost independent of the CO_2 density through the whole micellar regime. Note that we observed a strong dependence of the aggregation number f of the CO_2 density (Figure 5). However, the radius of the micelles is almost independent of the CO_2 density. This phenomenon is a direct consequence of the balance between the free energy of the corona (which depends on the excluded volume parameter) and the interfacial free energy (which depends on the core−corona interfacial tension γ.[28−31] The quality of the solvent for both the corona and core increases with the CO_2 density. The excluded volume parameter v for the corona chains increases with CO_2 density (see Table 1) and the core−corona interfacial tension γ decreases[32] (improving solubility) with density as shown in Figure 4. These

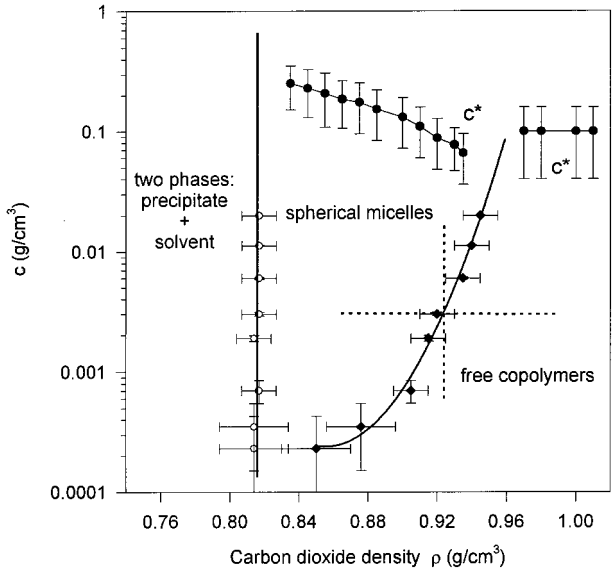

Figure 7. Phase diagram in the copolymer concentration−CO_2 density plane at a fixed temperature $T = 45$ °C. Points (○) represent the cloud line (solubility line), the points (♦) represent the spherical micelles−unimers transition, and the points (●) represent the overlap concentration c^*.

two effects compensate for each other and lead to almost constant size of the micelles as their aggregation number decreases with an increasing carbon dioxide density. Note that a decrease in the micelle size with an increasing density of supercritical fluids has been observed in experimental studies on surfactant systems.[11,33−35] But the micellization transition has not been observed in these studies. Also note that a decrease in micelle size with increasing density has been measured in neutron-scattering experiments and predicted theoretically for a microemulsions system.[33]

The size of the micelles (15.3 ± 1 nm) and of the unimers (4 ± 0.5 nm) is also almost independent of the copolymer concentration. In Figure 6 the size is obtained using the cumulant analysis. Upon increasing carbon dioxide density by increasing the pressure, we observe a very sharp transition from micelles to unimers.

Figure 7 shows the phase diagram in the CO_2 density−copolymer concentration plane at the fixed temperature $T = 45$ °C. The points corresponding to the transition in Figure 7 were deduced from the dynamic light-scattering experiments (dashed lines in Figure 6) and are reported as solid diamonds in Figure 7. From the comparison between Figures 6a, 6b, 6c, 6d, and 6e in the high CO_2 density region ($0.91 < \rho < 0.95$), we concluded that the micelles−unimers transition is shifting to the higher CO_2 densities with an increasing copolymer concentration (see the positive slope of the CMC line on the phase diagram plotted in Figure 7). Open circles indicate the cloud line (solubility line) determined by the cloud point and the light-scattering experiments. The solubility line which defines the transition between a two-phase regime and a micelles regime is almost independent of the copolymer concentration. The CMC line and the solubility line merge together at a very low copolymer concentration ($c \approx 2 \times 10^{-4}$ g/cm^3).

We have identified three regions on the phase diagram: a two-phase region at densities below 0.82 g/cm^3; a region of spherical micelles at intermediate CO_2 densities; a phase of isolated copolymer chains dissolved

in CO_2 at high densities. As the CO_2 density is increased, the solvent quality for both blocks becomes better, increasing the solubility of the PTAN and PVAC blocks in CO_2. To form micelles, more copolymer needs to be added to the solution. So the critical micelle concentration increases with increasing CO_2 density.

The dashed lines in Figure 7 represent the two different ways to reach the micelles-to-unimers transition. The critical micelle concentration is defined as the copolymer concentration at a given CO_2 density above which the formation of micelles is favorable. The transition can be observed as we increase the copolymer concentration (move up the vertical dashed line) at constant CO_2 density. In our experiments we have performed a density-driven micellization at a given copolymer concentration (see horizontal dashed line). This study is the first one reporting a density-induced transition between a spherical micelle phase and a unimer phase using light-scattering experiments.

The overlap concentration can be estimated from the density inside micelles.[23,24]

$$c^* = \frac{3fM_W}{N_A 4\pi {R_G}^3} \tag{25}$$

The radius of gyration R_G was too low to be measured using static light scattering. We have estimated it from the hydrodynamic radius R_H using the following approximate relation: $R_G = R_H/0.66$.[24,36] This relation was verified for random coils and is expected to still be valid for low-density micelles but is probably incorrect for dense micelles (large aggregation number at low CO_2 density). The experimental error bars were evaluated from the corresponding error bars in the measurement of hydrodynamic radii and aggregation numbers (see eq 25). The polymer concentration inside the micelles is quite high at low CO_2 densities but is in good agreement with other scattering studies.[23,26,27] Note that at fixed CO_2 density the variation of the polymer concentration inside micelles in the experimental concentration range is about 10%. The overlap concentration plotted in Figure 7 as solid spheres was estimated at different polymer concentrations for a given CO_2 density and extrapolated to a concentration $c = c^*$. The overlap concentration for unimers is found to be of the order of 0.1 g/cm^3. The expected decrease of c^* of unimers due to the change of the solvent quality is 17% (which is much smaller than the estimated error bar).

Above the overlap concentration c^* in the micellar phase, we expect microphases (i.e., lattices of micelles, cylinders, lamellae[37]). Note that experimental examples of density-tuning phase behavior of Aerosol-OT microemulsions in compressed liquids and of nonionic surfactants in light alkanes have been reported.[38,39]

Figure 8 shows a typical example of the results obtained by applying the Contin method to our data for a copolymer concentration $c = 3 \times 10^{-3}$ g/cm^3 at three different CO_2 densities. As we cross the micelles-to-unimers transition line (as we cross the solid line along the horizontal dashed line in Figure 7), we clearly distinguish one distribution in the region of spherical micelles at lower CO_2 density (Figure 8a), two distributions (micelles and unimers) at intermediate CO_2 density (Figure 8b), and one distribution at high CO_2 density (region of isolated copolymer chains, Figure 8c).

3.3. Micellization Transition. To study the micelles-to-unimers transition in more detail, we have

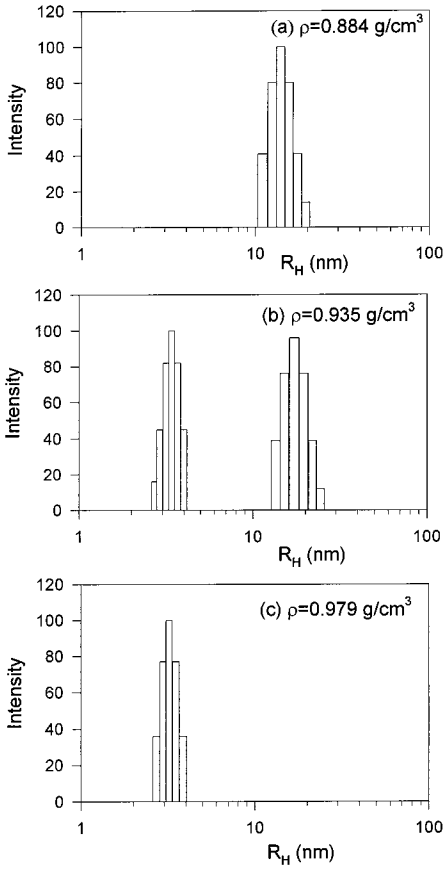

Figure 8. Intensity distribution obtained using the Contin method for copolymer concentration $c = 3 \times 10^{-3}$ g/cm^3 and CO_2 densities: (a) $\rho = 0.884$ g/cm^3, (b) $\rho = 0.935$ g/cm^3, and (c) $\rho = 0.979$ g/cm^3.

used the Contin distribution to evaluate the concentration of unimers and the concentration of micelles as a function of CO_2 density. To analyze these data, we applied the following procedure: Let the molecular weight of free copolymer chains and micelles be $M_{unimers}$ and $M_{micelles} = fM_{unimers}$ (where f is the aggregation number and $M_{unimers} = 70.7$ kg/mol). The corresponding concentrations of free unimers and unimers in micelles are $c_{unimers}$ and $c_{micelles}$, respectively. The total concentration of the solution c is equal to the sum of the concentrations.

$$c = c_{unimers} + c_{micelles} \tag{26}$$

The value of the total intensity I was deduced directly from the static light-scattering measurements.

$$I = I_{unimers} + I_{micelles} \tag{27}$$

The ratio r of scattering intensity of unimers $I_{unimers}$ to micelles $I_{micelles}$ can be measured independently using the Contin intensity distribution (see, e.g., Figure 8).

$$r = \frac{I_{unimers}}{I_{micelles}} \tag{28}$$

Consequently, the values for $I_{unimers}$ and $I_{micelles}$ can be calculated. From the scattering intensity of unimers $I_{unimers}$ we deduced the concentration of unimers:

$$c_{unimers} = \frac{I_{unimers}}{KM_{unimers}} \tag{29}$$

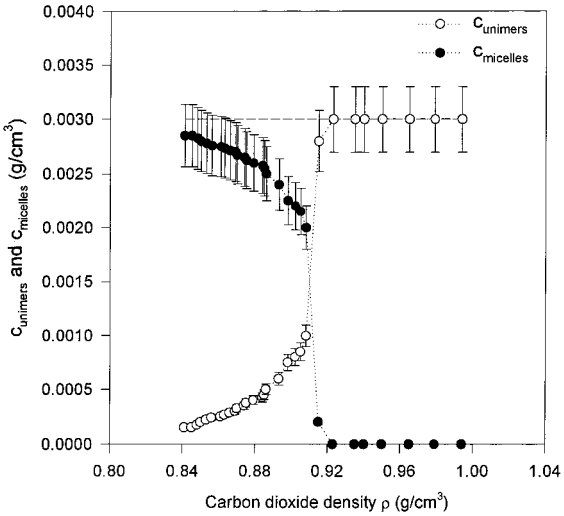

Figure 9. Dependence of the unimer concentration (○) and of the micelle concentration (●) on CO_2 density. The total copolymer concentration is $c = 3 \times 10^{-3}$ g/cm^3.

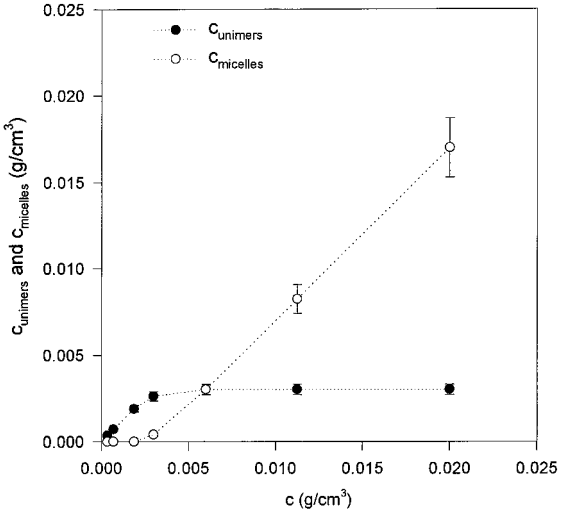

Figure 10. Dependence of the unimer concentration (●) and of the micelle concentration (○) on total copolymer concentration at the CO_2 density $\rho = 0.91$ g/cm^3.

where K is the scattering constant (see eq 3). From the concentration of unimers $c_{unimers}$ and the total concentration c, we calculate the concentration of the polymer in micelles $c_{micelles} = c - c_{unimers}$ (see eq 26).

The above procedure is applicable as long as we can distinguish the unimer scattering peak in the Contin intensity distribution. At CO_2 densities below the micelles-to-unimers transition in the micelle region, the unimer peak is not measurable and we cannot determine the unimer concentration. From the phase diagram plotted in Figure 7, we can approximate the concentration of unimers as a function of CO_2 density in the region of spherical micelles. In this part of the phase diagram we expect that the concentration of unimers to be of the order of the critical micelle concentration (CMC) for a given density. Figure 9 shows the variation of the concentration of unimers, $c_{unimers}$, and of micelles, $c_{micelles}$, as a function of CO_2 density for the total copolymer concentration $c = 0.003$ g/cm^3. For example, for the three CO_2 densities represented in Figure 8, this analysis gives the following results: for CO_2 density $\rho = 0.884$ g/cm^3, $c_{micelles} = 2.75 \times 10^{-3}$ g/cm^3 and $c_{unimers} = CMC = 3.5 \times 10^{-4}$ g/cm^3

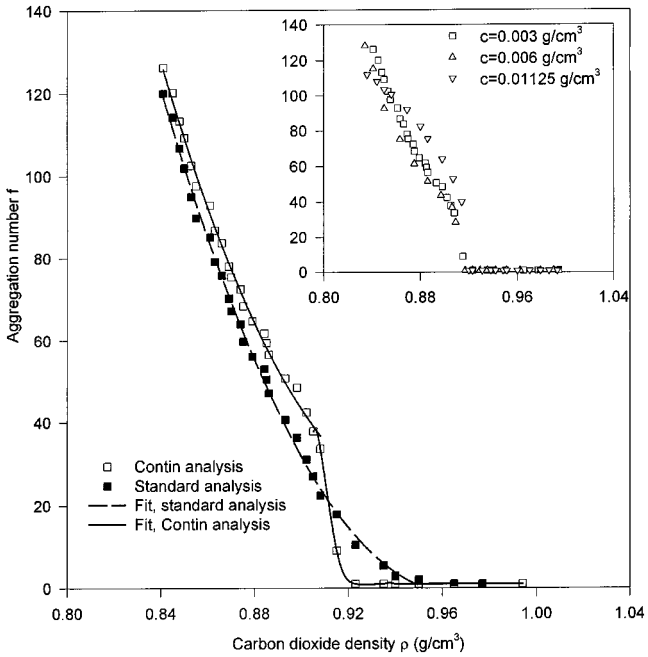

Figure 11. Variation of the aggregation number evaluated using the Contin analysis (□) and using the standard analysis (■) for a copolymer concentration $c = 0.003$ g/cm^3. The dependence of the aggregation number on the copolymer concentration obtained using the Contin analysis is plotted in the insert for copolymer concentrations $c = 3 \times 10^{-3}$, 6×10^{-3}, and 1.125×10^{-2} g/cm^3.

(Figure 8a); for $\rho = 0.935$ g/cm^3, $c_{micelles} \approx 0$ g/cm^3 and $c_{unimers} \approx 3 \times 10^{-3}$ g/cm^3 (within 10% experimental error) (Figure 8b); for $\rho = 0.979$ g/cm^3, $c_{micelles} = 0$ g/cm^3 and $c_{unimers} = c = 3 \times 10^{-3}$ g/cm^3 (Figure 8c). This plot shows that the micelles-to-unimers transition is very sharp. Most of the polymers are in the micelles below the transition and are unimers above the transition.

The concentrations of micelles and of unimers (deduced from the analysis described above) is plotted in Figure 10 as functions of the copolymer concentration for carbon dioxide density $\rho = 0.91$ g/cm^3. The concentration of unimers in the spherical micelles region is taken to be equal to the critical micelle concentration (equal to 0.003 g/cm^3 at CO_2 density $\rho = 0.91$ g/cm^3 (see Figure 9)). The unimer concentration is expected to saturate at the micellization transition and to be equal to the critical micelle concentration (CMC). The micelles appear at the transition and contain all the additional mass, $c_{micelles} = c - CMC$.

The aggregation number f deduced using this analysis at a copolymer concentration $c = 0.003$ g/cm^3 is presented in Figure 11.

$$f = \frac{I_{micelles}}{KM_{unimers}c_{micelles}} \tag{30}$$

The aggregation number obtained using the standard analysis (see part 3.1.3) is also plotted in the same figure. With improved analysis we are now able to define a sharp micelles-to-unimers transition. We reach the unimers phase for carbon dioxide densities around 0.91−0.92 g/cm^3 at a copolymer concentration of $c = 0.003$ g/cm^3. The dependence of the aggregation number on the copolymer concentration is shown in the insert in Figure 11. We observe a shift of the spherical micelles to unimers transition to higher CO_2 density when the copolymer concentration is increased.

4. Conclusion

We have presented the results of the light-scattering study of diblock copolymers in supercritical carbon dioxide.

We have identified three regions of the phase diagram (Figure 7) in the copolymer concentration−CO_2 density plane at the fixed temperature (T = 45 °C): (i) Two-phase region at low CO_2 density; (ii) spherical micelles at intermediate CO_2 density; (iii) unimers (isolated copolymer chains) dissolved in CO_2 at high density.

This is the first study reporting a density-induced (or a pressure-induced) transition between a spherical micelle phase and an unimer phase using light-scattering experiments.

The critical micelle concentration (boundary between phases (ii) and (iii)) increases with increasing CO_2 density (Figure 7). In our experiments, we have performed a density-induced micellization of block copolymers at several copolymer concentrations. This transition is driven by the important modifications of the selective solvent quality characteristics for the diblock copolymers induced by changing the density of CO_2. The analysis of the Contin intensity distribution shows that the micellization transition is very sharp (Figure 9).

We observed the decrease of the aggregation number with increasing CO_2 density, which is a direct consequence of improving solvent quality. The hydrodynamic size of the micelles was approximately constant through the whole region (ii). This can be understood by the compensation of the decreasing aggregation number and increasing excluded volume interactions inside the micelles. With the Contin analysis we are able to define sharp micelles-to-unimers transition (Figure 11).

We have also developed a technique to evaluate the interfacial tension between polydisperse PVAC homopolymers and CO_2 using GPC and static light-scattering data (Figures 3 and 4).

Acknowledgment. The authors gratefully acknowledge Prof. Benny D. Freeman for his help in the design of the high-pressure light-scattering setup and for interesting discussions and D. Betts for the synthesis of the homopolymers and diblock copolymers. The authors would like to thank the Kenan Center for the Utilization of CO_2 in Manufacturing for financial support.

References and Notes

(1) McHugh, M.; Krukonis, V. *Supercritical Fluid Extraction*; Butterworths: Boston, MA, 1986.
(2) DeSimone, J. M.; Guan, Z.; Elsbernd, C. S. *Science* **1992**, *257*, 945−947.
(3) Guan, Z.; Combes, J. R.; Elsbernd, C. S.; DeSimone, J. M. *Polym. Prepr. (Am. Chem. Soc., Div. Polym. Chem.)* **1993**, *34*, 447.
(4) Hoefling, T.; Stofesky, D.; Reid, M.; Beckman, E.; Enick, R. M. *J. Supercrit. Fluids* **1992**, *5*, 237−241.
(5) Guan, Z.; DeSimone, J. M. *Macromolecules* **1994**, *27*, 5527.
(6) Fulton, J. L.; Smith, R. D. *U.S. Patent 5,158,*704, Oct 27, 1992.
(7) Harrison, K.; Goveas, J.; Johnston, K. P.; O'Rear, E. A. *Langmuir* **1994**, *10*, 3536−3541.
(8) Hoefling, T. A.; Enick, R. M.; Beckman, E. J. *J. Phys. Chem.* **1991**, *95*, 7127−7129.
(9) Fulton, J. L.; Smith, R. D. *J. Phys. Chem.* **1988**, *92*, 2903−2907.
(10) Fulton, J. L.; Pfund, D. M.; McClain, J. B.; Romack, T. J.; Maury, E. E.; Combes, J. R.; Samulski, E. T.; DeSimone, J. M.; Capel, M. *Langmuir* **1995**, *11*, 4241−4249.
(11) Yates, M.; O'Neill, M. L.; Johnston, K. P.; Webber, S.; Canelas, D. A.; Betts, D. E.; DeSimone, J. M. *Macromolecules* **1997**, *30*, 5060−5067.
(12) Betts, D., Ph.D. Thesis, University of North Carolina at Chapel Hill, 1998.
(13) Hsiao, Y.; Maury, E.; DeSimone, J. M.; Mawson, S.; Johnston, K. *Macromolecules* **1995**, *28*, 8159−8166.
(14) Burns, R. C.; Graham, C.; Weller, A. R. M. *Mol. Phys.* **1986**, *59*, 41−64.
(15) St-Arnaud, J. M.; Bose, T. K. *J. Chem. Phys.* **1979**, *71*, 4951.
(16) Cummins, H. Z.; Pike, E. R. *Photon Correlation and Light Beating Spectroscopy;* Plenum Press: New York, 1974.
(17) Koppel, D. E. *J. Chem. Phys.* **1972**, *57*, 4814.
(18) Sovoná, H.; Procházka, J. *Ind. Eng. Chem. Res.* **1993**, *32*, 3162−3169.
(19) Provencher, S. W. *Makromol. Chem.* **1985**, *82*, 632.
(20) Smith, S. W.; Freeman, B. D.; Hall, C. K. *Macromolecules* **1997**, *30*, 2052−2057.
(21) Smith, S. W. Dynamical Properties of Chain Like Fluids: Computer Simulation and Experiment; Ph.D. Thesis, NCSU, 1995.
(22) McClain, J. B.; Londono, D.; Combes, J. R.; Romack, T. J.; Canelas, D. A.; Betts, D. E.; Wignall, G. D.; Samulski, E. T.; DeSimone, J. M. *J. Am. Chem. Soc.* **1996**, *118*, 917.
(23) Lairez, D.; Adam, M.; Carton, J. P.; Raspaud, E. *Macromolecules* **1997**, *30*, 6798−6809.
(24) De Gennes, P. G. *Scaling Concepts in Polymer Physics*; Cornell University Press: Ithaca, 1979.
(25) O'Neill, M. L.; Yates, M. Z.; Harrison, K. L.; Johnston, K. P.; Wilkinson, S. P.; Canelas, D. A.; Betts, D. E.; DeSimone, J. M. *Macromolecules* **1997**, *30*, 5050−5059.
(26) Jada, A.; Hurtrez, G.; Siffert, B.; Riess, G. *Macromol. Chem. Phys.* **1996**, *197*, 3697−3710.
(27) Calderara, F.; Riess, G. *Macromol. Chem. Phys.* **1996**, *197*, 2115−2132.
(28) Tuzar, Z.; Kratochvil, P. *Surf. Colloid Sci.* **1992**, *15*, 1.
(29) Halperin, A. *Macromolecules* **1987**, *20*, 2943.
(30) Halperin, A.; Tirrel, M.; Lodge, T. P. *Adv. Polym. Sci.* **1991**, *100*.
(31) Flory, P. *Principles of Polymer Chemistry*; Cornell University Press: Ithaca, NY, 1971.
(32) Harrison, Ph.D. Thesis, University of Texas, 1998.
(33) Peck, D. G.; Johnston, K. P. *J. Phys. Chem.* **1991**, *95*, 9549−9556.
(34) Johnston, K. P.; McFann, G.; Lemert, R. M. *Am. Chem. Soc., Symp. Ser.* **1989**, *406*, 140−164.
(35) Bartscherer, K. A.; Renon, H.; Minier, M. *Fluid Phase Equilibr.* **1995**, *107*, 93−150.
(36) Schmidt, M.; Burchard, W. *Macromolecules* **1981**, *14*, 210−211.
(37) McConnel, G. A.; Gast, A. P. *Macromolecules* **1997**, *30*, 435−444.
(38) McFann, G. J.; Johnston, K. P. *J. Phys. Chem.* **1991**, *95*, 4889.
(39) McFann, G. J.; Johnston, K. P. *Langmuir* **1993**, *9*, 2942.

MA980442J